Advanced evaluation of asphalt mortar for induction healing purposes

Apostolidis, P.; Liu, X.; Scarpas, A.; Kasbergen, C.; van de Ven, M. F C

DOI
10.1016/j.conbuildmat.2016.09.011

Publication date
2016

Document Version
Accepted author manuscript

Published in
Construction and Building Materials

Citation (APA)
Apostolidis, P., Liu, X., Scarpas, A., Kasbergen, C., & van de Ven, M. F. C. (2016). Advanced evaluation of asphalt mortar for induction healing purposes. *Construction and Building Materials*, *126*, 9-25. https://doi.org/10.1016/j.conbuildmat.2016.09.011

Advanced Evaluation of Asphalt Mortar for Induction Healing Purposes

P. Apostolidis[1], X. Liu[1], T. Scarpas[1], C. Kasbergen[1], M.F.C. van de Ven[1]

[1] Section of Pavement Engineering
Faculty of Civil Engineering and Geosciences, Delft University of Technology
Stevinweg 1, 2628 CN Delft, the Netherlands
Tel. +31 61 6599128, Email: P.Apostolidis@tudelft.nl

Corresponding author:
P. Apostolidis
E-mail: p.apostolidis@tudelft.nl

ABSTRACT

Induction heating technique is an innovative asphalt pavement maintenance method that is applied to inductive asphalt concrete mixes in order to prevent the formation of macro-cracks by increasing locally the temperature of asphalt. The development of asphalt mixes with improved electrical and thermal properties is crucial in terms of producing induction healed mixes. This paper studies the induction healing capacity of asphalt mixes without aggregates as the part of asphalt concrete where inductive particles are dispersed notably contributing to the final response of asphalt pavements. Special attention was given to the characterization of inductive asphalt mixes using experimental techniques and numerical methods. The research reported in this paper is divided into two parts. In the first part, the impact of iron powder as filler-sized inductive particle on the rheological performance of asphalt-filler systems was studied. The mechanical response, the induction heating and healing capacity of asphalt mortar by adding iron powder and steel fibers was evaluated as well. In the second part, the utilization of advanced finite-element analyses for the assessment of the induction heating potential of inductive asphalt mortar with steel fibers are presented. The influential factors of induction mechanism in asphalt mixes are also described. The experimental and numerical findings of this research provided an optimization method for the design of induction healed asphalt concrete mixes and the development of necessary equipment that will enable the implementation of induction technology for healing of asphalt concrete mixes.

1. Introduction

Asphalt concrete mixes are the most common types of pavement surface materials applied in transportation infrastructure and consist of asphalt binder, aggregate particles and air voids. These mixes are temperature-dependent materials with a self-healing capability because they can restore stiffness and strength (*1-5*). Nowadays, it is known that asphalt concrete mixes should be considered as mixes of mortar-coated aggregates rather than binder-coated aggregates in terms of developing asphalt pavements with enhanced durability. In 2014, the European asphalt industry (EU27) produced about 280 million tonnes of asphalt and invested about €80 billion per year in pavement construction resulting increased energy consumption and CO_2 emissions during various asphalt production, construction and maintenance processes (*6*). The importance of reducing CO_2 emissions by developing new, last longer asphalt mixes and to enhance road safety by providing high quality road network is crucial for fulfilling the European objective for sustainable development. Within this framework, the necessity of solving construction and rehabilitation issues of pavement structures has led industry to focus on development of alternative novel state-of-the-art techniques. Regarding asphalt pavement maintenance, among others (*7, 8*) healing of asphalt micro-cracks using the induction technique has been approved as a very promising method to prolong the service life of asphalt pavements (*9-13*).

The induction heating technique has been used as a maintenance technique for asphalt pavements in order to speed up the healing process of asphalt. Field trials are available and a very exciting example is the Dutch motorway A58 near Vlissingen (*14*). This technique requires new mixes with inductive particles in order

to make them suitable for induction heating. Specifically, when an alternating electric current is applied to an induction coil, a time-variable magnetic field is generated around the coil. According to Faraday's law, this magnetic field induces currents (eddy currents) in inductive particles within the mix and they are heated up based on the principles of Joule's law. The generated heat in particles increases locally the temperature of asphalt mix around the stone aggregates, rather than heating them. Through the temperature rise the bitumen is melting the micro-cracks are closed and the mechanical properties are recovered (*4*). This mechanism of healing asphalt mixes with the assistance of electro-magnetic induction is known as induction healing.

Previous research indicated that asphalt mixes with inductive particles, such as steel fibers, can be heated in a very short time by using the induction technology (*9-17*). However, the distribution of steel fibers within mixes appears to have a direct relation with the volumetric and mechanical properties of asphalt mixes(*18-21*). Also, it was observed that the characteristics of steel fibers – diameter and length - are affected by the mixing and compaction processes (*16*). Especially, the longer steel fibers easily produce clusters inside the asphalt mixes, causing inhomogeneity and reducing the mechanical response (*15, 16*). Apart from the performance degradation, the large amounts of fiber-type particles cause a significant increase of costs (*28*). For this reason and in order to resolve the problems resulted by the fiber-type particles, inductive asphalt concrete mixes can be produced by adding other types of inductive components.

In particular, the effective properties of asphalt mixes vary considerably according to the type and the characteristics of inductive particles. Higher electrical or thermal conductivity of particles results in higher effective conductivities of the asphalt concrete mixes. These particles are normally divided into categories according to their size and shape as: filler-sized (e.g., graphite, carbon black) (*11, 32-36*), stone-sized (e.g., steel slag) (*31*) and fiber particles (e.g., steel and carbon fibers) (*11, 36, 37*). Among all the fillers used in inductive asphalt mixes, carbon black and graphite powder are the most often investigated because of their excellent associated compatibility with asphalt binder imparting in parallel easy mixing. However, no extended research has focused on other types of filler-sized inductive particles and for this reason is presumed very important to develop inductive mixes with well dispersed inductive components to provide sufficient isotropic material properties to mixes for induction applications.

Additionally, more data is still required to clarify the role and the significance of the various parameters on the asphalt induction heating phenomenon. Induction heating is a complex phenomenon that combines the electromagnetic and heat transfer theory and has a strong relationship with the electro-thermal properties of materials (*22-24*). Furthermore, it is known that the efficiency of the induction heating depends on the coupling between the size of the inductive particles and the operational characteristics of the induction coil (frequency, power, shape of the induction coil, etc.). Thus, the experimental and the numerical analysis of electro-thermo-mechanical properties of asphalt mixes is becoming very important in terms of determining the most crucial material parameters for obtaining enhanced durability simultaneously with high induction heating rate.

This paper is divided into two investigation approaches; the experimental and the numerical. Since asphalt mortar is the crucial part of asphalt concrete that suffers more damage and contains the particles for induction heating, an experimental approach was developed for the sufficient characterization of structural and non-structural performance of induction heated mortars. The current numerical study provides us this efficient tool to conduct analysis of induction heating predicting in parallel the heating time needed in order to heal micro-cracks inside the asphalt mixes.

2. Experimental Approach

During the induction heating, the asphaltic part around the stone aggregates with the inductive particles is heated locally resulting durability improvement of the bonding characteristics between asphalt constituents. In this study focus was given on conducting in-depth analyses of the interaction between the inductive particles with the other asphalt constituents. Also the evaluation of structural and non-structural performance of asphalt mastics (binder and filler-sized particles) and mortars (binder, filler-sized particles and sand) was ascertained crucial.

Iron powder was selected as filler-sized particle and its interaction with the other components was studied on asphalt mastic level. For a certain asphalt binder, asphalt mastics with different volumetric properties were developed and characterized following an experimental protocol designed for this purpose. It is well recognized that the performance of asphalt mastic is associated with reinforcement of filler-sized particles in asphalt mastic (*38-40*). The particle size of filler, the loading time, temperature and the interaction of fillers within the binder matrix are the most influential factors for the stiffening of mastics. Rheological and micro-morphological analyses were carried out quantifying thus the stiffening potential of iron powder with different contents. The electro-thermal properties were assessed within an effort to obtain the optimal combination of fillers in this study.

After the completion of mastic characterization, sand and steel fibers were added in asphalt-filler systems in order to prepare the inductive asphalt mortars. The effect of different volumes of fibers and powder on the electrical conductivity of mortar was evaluated by using the same experimental technique with the mastic level of analysis. Once the optimal inductive particles combination was obtained, the thermal conductivity of inductive asphalt mortars was studied. Due to the fact that the improved macroscopic response of asphalt pavements has a direct link with the durability of asphalt mixes, the mechanical performance of asphalt mortars were investigated as well. Although the reinforcing impact of steel fibers on mechanical properties of asphalt mixes has been studied extensively, still limited research was done to evaluate the performance of asphalt mortars with different inductive particles. At the end of the experimental analysis of this paper, the induction heating and healing capacity of inductive asphalt mortars were examined.

2.1 Material and preparation

Firstly, the selected mineral fillers and the iron powder as filler-sized inductive particle were analyzed. A scanning electron microscope (SEM), BET (Brunuer, Emmett and Teller theory) and a Ultrapycnometer have been utilized in order to determine shape, specific surface area and density, respectively. **Fig. 1** shows the SEM images of the filler-sized particles; weak limestone (WL) filler, produced limestone (PL) filler and iron powder (IP). It can be seen that the angular shape and the size of filler limestone – WL and PL – is similar compared with iron powder (IP) where it has slightly smaller size and smoother surface texture than the minerals.

In order to investigate the impact of iron powder as filler-sized particle within the asphalt mastic, two asphalt-filler preparation processes were used. The first one was by adding iron powder with replacing an equivalent volumetric amount of mineral fillers and the other one was without replacing the mineral fillers. It is important to note that the addition order of fillers, the mixing time and the mixing temperature affect the dispersion, the segregation and probably the agglomeration of fillers in the mastics. In order to avoid the settlement of iron powder due to its high density, a preliminary mixing processing analysis was conducted using a X-ray nano-CT scanner. It was concluded that the lowest air void content and iron powder settlement was seen when the mixing sequence was the following; (1) addition and mixing of filler-sized particles together for 90 sec and (2) addition of asphalt binder which is SBS polymer modified and mixing it together with particles for 120 sec. Mixing was carried out at 180 ^{o}C. The compositions of the different inductive asphalt mastics (F().P()) are given in Table 1. The notation F indicates mineral filler and P represents iron powder. The values in the brackets indicate the corresponding volume of the components.

After the performance evaluation of asphalt mastics, inductive asphalt mortar was developed. The weight percentage of components in the original asphalt mortar was 33%, 5%, 34% and 28 % for mineral filler WL, PR, sand and asphalt binder, respectively. For the development of asphalt mortar, steel fibers (SF) (7756 kg/m^3, initial length 2.5 mm and diameter 0.083 mm) were mixed with the other components as volume percentage of asphalt binder. Also, in this level of study, the inductive mortars were prepared with different volume percentages of iron powder added after substituting the equivalent volumetric part of mineral fillers in order to avoid volumetric degradation. The final optimal amount of iron powder in asphalt mortar was determined from the electrical conductivity measurements. This specific amount was used for the further experimental investigations. Initially, different combinations of steel fibers were mixed to obtain the

percolation threshold. Later, iron powder of 5%, 10%, 15%, 20% and 25% was added and the amount of steel fiber by volume of bitumen was kept constant (4%).

2.2 SEM Imaging

Micrographs of the inductive asphalt mastics were captured using a scanning electron microscope (SEM). The micrographs were obtained from a JEOL JSMM 6500F using an electron beam energy of 15 keV and beam current of approx. 100 pA. The backscattered electron image mode (BSE) was selected for the image acquisition. Aluminum cylinders with a height of 18 mm and a diameter of 31 mm were used as sample-substrates for SEM scanning. A thin film of mastic was applied on a glass plate at 140 ^{o}C in order to form a very smooth area at one side after which the sample was stored at room temperature for 24 hours. Then, the sample was gently cut and placed on the aluminum cylinders. The study of micro-morphology of asphalt mastic was performed in environmental mode.

2.3 Frequency sweep test

Dynamic shear rheometer (DSR) was utilized to obtain the rheological properties of the inductive asphalt mastic. Frequency sweep tests were carried out over a temperature range of -10 ^{o}C to 60 ^{o}C and the complex modulus and phase angle were determined. By shifting these mechanical properties to a reference temperature (i.e. 30 ^{o}C), the master curves of the complex modulus and phase angle were built up for all inductive mastics. Before starting frequency sweep tests, a stress sweep test was conducted in order to identify the material linear viscoelastic range (LVR). The LVR is characterized as the 10% stiffness reduction criterion and was used to filter the linear and non-linear viscoelastic region.

2.4 Determination of electro-thermal properties

After the preparation of the inductive asphalt mixes, the material was poured in silicon-rubber mould, to obtain samples with rectangular dimensions 125 × 20 × 25 mm. The electrical resistivity measurements were done by performing the two-electrode method at a room temperature of 20 ^{o}C. In order to avoid the problem of binder concentration at the surface of contact area and to achieve sufficient and low resistance contact with the electrodes, the short ends of specimen are cut by 1mm and a very thin silver paste was glued at both ends. The electrodes were made of copper, placed at both sides and the electrical volumetric resistance was measured using a digital multimeter. In the experimental measurements, the electric field and the contact resistance between the electrodes and the mix was considered constant and zero respectively.

The geometry and the electrical resistivity of the inductive asphalt mastic and mortar are the only parameters that influence the electrical resistance. The difference in potential value between the electrodes and their total charge do not play a role for this material property. Therefore, the electrical resistivity was obtained from the second Ohm's law as follows:

$$\rho = \frac{RS}{L} \tag{1}$$

where ρ is the electrical resistivity, measured in Ωmm, L is the internal electrode distance, measured in mm, S is the electrode conductive area measured in mm^2 and R is the measured resistance, in Ω.

Thermal conductivity measurements were performed by using the C-Therm TCi thermal analyzer, **Fig. 2**. The thermal sensor was working according to the Modified Transient Plane Source Method to determine the thermal resistivity of asphalt mixes. The material was poured in a conical-shaped mould with height of 15 mm and top and bottom diameter of 50 mm and 55 mm, respectively. The sensor was heated by a small current and the response was monitoring while in contact with the specimen. The thermal resistivity of the specimen

were measured and obtained directly from the sensor. From the inverse of the resistivity the conductivity is defined as:

$$q = -k \cdot \frac{dT}{dx} \quad (2)$$

where q is the heat flux (the amount of thermal energy flowing through a unit area per unit time), dT/dx is the temperature gradient and k is the coefficient of thermal conductivity, often called thermal conductivity. The heating, reading and cooling process was repeated 6 times per specimen to obtain an average of the reading. For both electrical and thermal measurement, three replicas were used.

2.5 Mechanical performance

In order to investigate the impact of inductive particles on the mechanical properties of the asphalt mortar, direct monotonic tensile tests were carried out. A 25 kN electro-hydraulic servo testing machine was used and the monotonic tension tests with freely rotating hinges were performed on specimen from inductive asphalt mortar. In order to reduce undesired eccentricities, the specimen were carefully positioned in the special designed steel hinges. Furthermore, the inductive asphalt mortar specimen had a parabolic geometry, **Fig. 3**, with height of 34 mm for the parabolic part and a thickness of 10 mm in the middle. The monotonic tension tests were performed at different displacement rates. The fatigue performance was tested in load control mode. All tests were carried out at a constant temperature of -10 ^{o}C.

2.6 Induction heating

The induction heating experiment was performed with a 550 V RF generator 50/100 (Huttinger Electronic, Germany), see **Fig. 4**, at a maximum frequency of 63.5 kHz. The distance from the mortar sample (125 × 20 × 25 mm) to the coil was 10 mm and the data were obtained from the surface of the specimen by using an infrared (IR) thermometer.

2.7 Induction healing

In order to determine the healing efficiency of asphalt mortar after mixing inductive particles, asphalt mortar beams were produced with dimensions 105 × 25 × 13 mm in a mould with a notch at the middle. A similar experimental procedure as proposed by Liu et al (*12*) was selected to test the healing capacity of the asphalt mortar. The sample was placed in a chamber at -10 ^{o}C and was broken into two pieces using the three point bending setup. The two pieces were then placed back into the mould. At the final stage, the two pieces were heated via induction energy until the surface temperature reached 120 ^{o}C. This process was continued after resting the sample for 2 hours at 20 ^{o}C. Moreover, this process was repeated until the damage was too high to continue the healing process (*12*). Concerning the temperature, -10 ^{o}C was chosen in order to avoid permanent deformation of the material and to obtain a brittle fractured surface. For the induction healing analysis, 5 samples were used for each type of inductive mortar.

The induction healing performance was evaluated by using the relation given below:

$$S(t) = \frac{F_i}{F_0} \quad (3)$$

where F_0 is the fracture force of the sample during a three point bending test, and F_i is the fracture force after the induction heating.

3. Numerical Approach

As previously described, inductive particles are required into the asphalt mixes in order to make them suitable for induction heating. Addition of inductive fibers is much more effective than to add inductive filler-sized particles (*11*) and also the volume of these and binder influences the induction heating efficiency (*13*). Also, it has been observed that the thermal and the electrical conductivity as well as the induction heating efficiency are dependent of the volume of fibers in asphalt mixes (*15*). Consequently, apart from the operational conditions – frequency, intensity of the magnetic field, etc - the efficiency of this type of electromagnetic heating is dependent on the effective properties of the asphalt mixes with inductive fibers and other particles.

However, still limited research was conducted to quantify the influence of different operational parameters of an induction system on heating efficiency of asphalt mixes. The second part of this paper studies the important factors of induction heating in asphalt mortar mixes. The 3D finite element meshes of asphalt mortars with different volumes of steel fibers were generated using X-ray scans in order to evaluate the effective electrical and thermal properties. After the numerical determination of important induction parameters for the inductive asphalt mortar, a 3D finite element model of electromagnetic phenomena coupled with heat transfer physics was developed.

3.1 Finite element meshes of asphalt mortar

Previous researches (*13, 15*) indicated that, by adding inductive particles (e.g., steel fibers), an asphalt mix can be heated up in a very short time by using the induction technology. In order to simulate the effective electrical and thermal properties of inductive asphalt mixes, the 3D finite element meshes of inductive asphalt mortars - as a representative of the asphalt mixes without stone aggregates - with different volumes of steel fibers were generated by using High-resolution X-ray CT (Computed Tomography) images.

The High-resolution X-ray CT is a completely non-destructive technique for visualizing features in the interior of opaque solid objects, and for obtaining digital information on their 3D geometries and properties. By the X-ray CT technology, the different densities of individual components (e.g., sand, filler, air voids and bitumen) in the asphalt mortar can be distinguished by the gray levels in a CT slice.

Simpleware software (*27*) was utilized to comprehensively process 3D image data and to generate volume and surface meshes from the image data. Meshes can be directly imported into the COMSOL multiphysics finite element software for the electrical and thermal conductivity analyses. The process of reconstruction of 3D images of inductive asphalt mortars is illustrated in **Fig. 5**.

3.2 Finite element models and parameters

A finite element model predefined in the COMSOL software (*25, 26*), which can simulate electro-magneto-thermal phenomena in a real time system, has been utilized for modelling induction heating in the asphalt mortar. The electromagnetic field was modeled by means of the magnetic field intensity vector **A** [A/m^2] and the magnetic flux density vector **B** [A/m] as shown in equation 4:

$$(j\omega\sigma - \omega^2\varepsilon_0\varepsilon_r)\mathbf{A} + \nabla \times \left(\frac{1}{\mu_0\mu_r}\mathbf{B}\right) - \sigma\mathbf{v} \times \mathbf{B} = {J_\varphi}^e \quad (4)$$

where j denotes the imaginary unit, ω the angular frequency of the harmonic current, σ is the effective electrical conductivity, ε_0 is the electric permittivity of vacuum ($8.854 \cdot 10^{-12}$ As/Vm), ε_r is the relative electric permittivity, μ_0 is the magnetic permeability of vacuum ($4\pi \cdot 10^{-7}$ Vs/Am) and μ_r is the relative permeability.

The model was created by using a Single-Turn Coil domain feature and the governing equation of the induction coil under frequency-transient study analysis is given by:

$$I_{coil} = \int_{\partial\Omega} \mathbf{J} \cdot \mathbf{n} \quad (5)$$

where I_{coil} denotes the flowing current of the coil.

Finally, the heating equation governed by the Fourier heat transfer equation is defined by:

$$\rho c_p \frac{\partial T}{\partial t} + \rho c_p \mathbf{u} \cdot \nabla T = \nabla \cdot (k \nabla T) + Q \quad (6)$$

where ρ is the density, c_p is the specific heat capacity, k is the thermal conductivity, T is the temperature and Q is the energy generated in the asphalt mixture per unit volume and time.

For the assessment of the influence of induction coil operational conditions on the induction heating potential of the inductive asphalt mortar, a finite element (FE) model was developed. The model makes use of one induction coil at a distance of 50 mm above the surface of the mortar sample, **Fig. 6.a**. The induction coil with a square cross-section of side 0.1 m was assumed. By imposing the alternative current to the coils, eddy current can be generated in the vicinity of the inductive asphalt mortar. It should be noted that the geometry of the induction coil has significant impact on the induction heating efficiency (*29, 30*). For this reason, the higher order tetrahedral elements were utilized to model the coil and the entire induction system, **Fig. 6.b**. In addition to the coil, the model consists of one layer of the inductive asphalt mortar with a thickness of 30 cm, one layer of ground sand soil underneath the mortar layer and air above the mortar layer. Normally the electro-thermal properties of inductive asphalt mixes are temperature dependent. However, for simplicity, the electro-thermal properties of the inductive asphalt mortar were assumed constant in the simulations.

In order to make the asphalt mortar inductive, it was assumed that 6% of steel fibers was added into the asphalt mixture. The electrical and thermal conductivity of the inductive asphalt mortar were taken from the numerical analysis as well. Furthermore, in the following numerical simulations, the parameters of the relative permeability and heat capacity of the inductive mortar were assumed to be 1 and 920 J/(kg·K) respectively. Moreover, an ambient temperature of 20 ^{o}C was assumed to simulate the induction heating operation at normal environmental conditions. The duration of induction heating simulation was 120 seconds. The applied power voltage and the frequency of the alternating magnetic field were set to 550 V and 64 kHz for the simulations based on the experimental experience in the first part of this paper.

4. Results

4.1 Experimental results of asphalt mastics

4.1.1 Micro-morphological images

The surface micro-morphology of asphalt mastic with iron powder is presented in **Fig. 7.a**. The different inductive asphalt mastics with different amounts of iron powder as described in Table 1 are investigated. The grey particles represent the mineral fillers and the brightest parts of the images are the iron powder. By comparing images 3 and 5 in **Fig. 7.b**, it is obvious that the inductive asphalt mastics without substituting the mineral filler - image 3 - appear to have a surface morphology with less dark space than asphalt mastics produced with substituting mineral filler with iron powder, image 5. The spacing among the filler-sized particles is reducing with increasing the amount of iron powder without substituting relative volumetric amount of mineral filler, images 1 to 3. Observation of inductive asphalt mastics surfaces with SEM images shows that the morphology of mastics after adding iron powder has a direct link with the concentration of filler-sized particles – iron powder and mineral fillers. It should be noted that the current micro-morphological results agree with the rheological results of inductive asphalt mastics which will be explained in the Frequency Sweep Test subsection.

4.1.2 Frequency sweep test

Before the frequency sweep tests, the stress sweep test was conducted from -10 ^{o}C to 60 ^{o}C with a shear stress range from 0.01 to 10 Pa and at 1 Hz in order to identify the linear viscoelastic range (LVR). The LVR is characterized as the 10% stiffness reduction criterion and was used to filter the linear and non-linear viscoelastic region. Afterwards, the frequency sweep test was carried out over a temperature range from -10 ^{o}C to 60 ^{o}C. At a reference temperature of 30 ^{o}C, the master curves as given in **Fig. 8** show the rheological behavior for all the inductive asphalt mastics. **Fig. 8.a** is the complex modulus as a function of frequency with respect to different inductive asphalt-filler systems and **Fig. 8.b** is the corresponding phase angle as a function of frequency as well. The test stress sweep and frequency sweep were run on 8 mm parallel plates with a 2 mm gap for mastics at all the testing temperatures.

The asphalt mastic without adding iron powder is obviously much stiffer than the inductive mastics produced after replacing mineral filler with iron powder. From **Fig. 8.a** it can be seen that the complex modulus of mastic F100.P50 is significantly higher than the mastic F50.P50 which has the same amount of iron powder. Apart from the higher complex modulus, the inductive mastics have lower phase angle when iron powder is added without replacing the mineral filler, **Fig.8.b**. The reducing visco-elastic properties at higher concentrations of filler-sized particles and when particles are added without substitution are linked with the interaction between the fillers of different shape and surface characteristics. These phenomena can be explained by the fact that the surface of iron powder is slightly smoother than the other mineral fillers and thus is easily rolling under shear stresses when is added in the binder matrix by replacing mineral filler. Also, increasing the concentration of filler-sized particles leads to lower the spacing among the particles within the binder matrix and asphalt mastics with lower viscosity and higher stiffness are obtained. Consequently, the stiffening potential of the different filler-sized particles and the asphalt-filler processing methods result direct effects on the mastic's workability and subsequently on the durability of asphalt mixes.

4.1.3 Electrical and thermal properties

The electrical resistivity of asphalt mastic decreases with increasing iron powder content with or without replacing an equivalent proportion of mineral filler, **Fig. 9**. In **Fig. 9.a**, a reduction of the electrical resistivity is observed when iron powder is mixed proportionally within the asphalt mastic by substituting mineral filler. Moreover, **Fig. 9.b** shows that the resistivity was also reduced after adding extra iron powder into the asphalt mastic matrix. The tendency of the electrical resistivity drop can be explained by the percolation threshold theory. The percolation threshold was reached when the shorter conductive pathways were formed by the higher amount of iron powder in the asphalt mastic. The inductive asphalt mastic F85.P15 represents the mastic at the percolation threshold position and adding more iron powder hardly reduces the electric resistivity further.

Additionally, the thermal conductivity of asphalt mastics produced, with and without substituting part of the mineral filler with iron powder, are presented in **Fig. 9**. It was found that the thermal conductivity of asphalt mastic increased after adding iron powder. The resulting increase is due to the thermal properties of iron which is added into the mastic. It is known that the thermal conductivity of iron powder is considerably higher than the conductivity of the other asphalt components. Hence the increase of the amount of iron powder leads to an increase of the effective thermal conductivity of the inductive mastic. This can be seen in **Fig. 9.a&b** showing that the thermal conductivity of sample F85.P15, which represents the inductive asphalt mastic at the electrical percolation threshold, was 0.56 W/mK. Also, the thermal conductivity of F85.P15 was higher than of pure asphalt mastic F100.P0 which was 0.487 W/mK.

The asphalt mastics without replacing of mineral fillers with iron powder show a lower electrical resistivity than those developed after replacement. This observation can be explained by the fact that the filler-sized particles form a dense skeleton with very short spacing between the particles when extra iron powder is added in the asphalt mastic. Moreover, the produced inductive mastics without substitution of mineral filler-sized particles had a higher thermal conductivity. At higher filler-sized particles concentration, the interaction among the particles is increasing within the asphalt mastics. Thus, the spacing among the particles and the coating role of asphalt binder around the particles reduces having as consequence this thermal observation for the inductive asphalt mastics.

4.2 Experimental results of asphalt mortars

4.2.1 Electrical and thermal properties

The change of the electrical resistivity of an asphalt mortar with steel fibers, but without iron powder is shown in **Fig. 10.a**. The conductive paths formed by steel fibers develop and lead to a gradual decrease of the resistivity above 2% volume of fibers. It is clear that the increase of the volume of steel fibers reduces the resistivity or increases the electrical conductivity of mortars. The optimum steel fibers content reached when no longer increases the electrical conductivity by adding more than 6.4% of steel fibers. For adding iron powder in the mortars with constant steel fibers content, it was selected asphalt mortar with 4% of steel fibers as a inductive mortar with amount of steel fibers beyond the percolation threshold.

The combination of steel fibers and iron powder further reduces considerably the electrical resistivity of the asphalt mortar, **Fig. 10.b**. It can be seen that, by choosing asphalt mortar with 4% of steel fibers and adding the iron powder stepwise in parallel with the reduction of mineral filler, the replacement of mineral filler with iron powder decreases the electrical resistivity of the asphalt mortar further. The optimum combination of particles in the asphalt mortar is 4% of steel fibers and 15% of iron powder. The amount of iron powder required to obtain the optimum combination of particles and according to the percolation threshold theory the shorter conductive pathway coincides with the previous observations at the mastic level. This volume combination of steel fiber and iron powder will be used for the further steps of this research.

For composite materials such as asphalt mixes, the effective properties can be determined by the proportion, the dispersion and the properties of individual components in the final material. By increasing the proportion of a component in the mix, the thermal conductivity of the final mix can be increased or decreased depending on the type and the nature of the component. In case of adding steel fibers. it is observed that the effective thermal conductivity of asphalt mortar increases with the additions of fibers, **Fig. 11**. Due to the fact that the thermal conductivity of steel fiber is quite high, when the volumetric part of steel fibers into the asphalt mortar is increased or decreased, the effective conductivity of the whole mix will increase or decrease respectively. The increase of thermal conductivity is slightly higher in the case of asphalt mortars mixed with both iron powder and steel fibers.

4.2.2 Direct tensile strength and fatigue performance

The direct tensile strength and fatigue tests provide crucial information about the impact of particles on the mechanical performance of the inductive asphalt mortar. The asphalt mortar is the first decentralized system of an asphalt mix and represents the matrix of the mix between the aggregates. This implies that the mechanical behaviour of mortar has a direct effect on the behaviour of mixes on pavements. The typical stress-strain curves at low temperatures (-10^{o}C) and at different displacement rates are presented in **Fig. 12**. It is obvious that the amount of steel fibres influences the maximum tensile stress. The tensile strength of the mortar increases with increasing fibre content. Therefore, the reinforcing effect of fibres on the asphalt mortar is apparent in **Fig. 12.c**, where the average values of the maximum tensile stresses are presented.

The effect on brittleness and ductility of the inductive asphalt mortar can be observed in **Fig. 12**. At high displacement rates, all samples show brittle response. More ductility can be observed for lower fiber contents and lower displacement rate. Particularly, the replacement of a part of mineral filler with iron powder, it does not influence significantly on the tensile strength of the asphalt mortar and the reinforcing effect of fibers.

In order to study the fatigue response of mortars with different combinations of inductive particles, a cyclic sinusoidal load is utilized. The magnitude of the loading is defined as the 40% of the ultimate tensile strength (0.3 kN). The loading frequency was 5 Hz and all the tests were carried out at -10 ^{o}C.

It can be observed that all asphalt mortar samples show the tertiary phase of deformation after certain loading time, **Fig. 13.a&b**. Particularly, by increasing the amount of steel fibers within mortar from 0% to 4%, the tertiary phase is significantly delayed and the fatigue life increases. Moreover, the fatigue life is extended

when steel fibers were added from 4% to 6% within the asphalt mortar. It can be seen that the asphalt mortar with 15 % of iron powder appear slightly higher fatigue life than the one without iron powder, **Fig. 13.c**.

4.2.3 Induction heating performance

In order to investigate the induction heating efficiency of the inductive asphalt mortar, at ambient temperature (20 ^{o}C), the test samples were heated for 120 seconds by the induction unit. The test samples were mixed with different volumetric combinations of steel fibers and iron powder. **Fig. 14** presents the average temperature at the top surface of samples at 120 seconds induction heating. It can be observed that the maximum surface temperature is related to the volume of steel fibers added in the asphalt mortar. The higher amount of fibers in the mortar sample led to the higher surface temperature and hence the higher induction heating efficiency of mortar. However, the increasing tendency of induction heating efficiency is not linear. For example, after 6% of fibers added in the mortar, the tendency of increasing temperature is not significant and it is stabilized. It means that mortars achieve the induction heating saturation limit where all the conductive paths are linked.

Similar observation can be found for the samples mixed with both iron powder and steel fibers. It can be seen that the induction heating efficiency can be enhanced by combination of iron powder and steel fibers into the asphalt mortar. The average surface temperature of the samples with 15% iron powder is higher than the samples without powder.

4.2.4 Induction healing performance

The induction healing efficiency of asphalt mortar with steel fibers is presented in **Fig. 15.a**. The cracks were healed by induction heating. However, after the first healing cycle, the strength was recovered by 60% of its original strength. This phenomenon can be explained by the loss of reinforcing effect of steel fibers in mortar (*17*). Apart from the induction healing of mortar, the use of steel fibers offers a reinforcing matrix with a network of random oriented fibers. However, when mortar is fractured, the interconnection among the fibers at the cracked surfaces is lost and mechanical performance of inductive mortar is as a material without fibers. In the second and third cycle, the strength recovery remained approximately constant. In the fourth cycle, material lost its strength completely. After several fracture - healing cycles, the cracked surfaces of fractured mortars were covered mostly by asphalt binder without steel fibers. As a result, the diffusion of binder from the one side of surface to the other was prohibited and subsequently the closure of crack of asphalt mortar. The fracture - healing process was continued successively in six cycles. Similar to the case of mortar mixed with fibers, the combination of steel fibers and iron powder can provide the same induction healing capacity to mortar, **Fig. 15.b**.

4.3 Numerical results of asphalt mortars

4.3.1 Numerical analysis of effective material properties

For the determination of electro-thermal properties of the inductive asphalt mortar, it is necessary to predefine the properties of individual components in the asphalt mortar. Therefore, in this investigation, the magnitudes of the electrical and thermal conductivity of the bitumen, mineral filler and sand were assumed to be $9 \cdot 10^{-5}$ S/m and 0.5 W/(m·K) respectively and for steel fiber $20 \cdot 10^{3}$ S/m and 16 W/(m·k) were assumed (*25, 26*). The 3D images of the asphalt mortars with different steel fibers contents are presented in **Fig. 16** and their effective electrical and thermal conductivities are determined numerically and given in **Fig. 17**.

The results in **Fig. 17** indicate that the electrical conductivity of the asphalt mortar increased with increasing the content of steel fiber. As it can be noticed, the electrical conductivity of the asphalt mortar increases rapidly when the volume fraction of the steel fiber is close to 6%. The reason of this dramatic increase of the electrical conductivity can be explained by the percolation threshold theory. The percolation threshold is reached when the shorter conductive pathways are formed by the higher amount of steel fibers in

the asphalt mortar. Similarly, it can be observed that, with the stepwise increase of steel fibers in the asphalt mortar, the effective thermal conductivity of the inductive asphalt mortar is increased from 0.71 W/(m·K) to 1.58 W/(m·K). This happened because the thermal conductivity of steel fibers is higher than the other components in the asphalt mortar.

According to the current numerical analysis, the improvement of effective electrical and thermal conductivity is dependent on the proportion of steel fibers in the asphalt mortar. Moreover, it is well known that it is difficult to obtain experimentally precise conductivity results from asphalt mixes (*28*). Therefore, this method of numerical analysis of asphalt mortar properties could be proved an effective tool to determine the electro-thermal characteristics of inductive asphalt mixes. Subsequently, understanding the conductivity mechanism is also another advantage of this numerical technique where the transformation phenomenon of asphalt mix, from insulator to conductor, can be quantified by identifying the percolation threshold limit.

4.3.2 Numerical analysis of induction heating

Effect of Material Properties

The numerical simulations for the one coil system were carried out first. The distribution of magnetic flux density and temperature on the inductive asphalt mortar are shown in **Fig. 18**. The influence of the electrical conductivity on the temperature distribution within the cross-section of the asphalt mortars is shown in **Fig. 19**. It should be noted that the asphalt mortar with 100 S/m of electrical conductivity corresponds to the response of the asphalt mortar mixed with 6% of steel fibers. Hence, the asphalt mortar with 1 S/m of electrical conductivity represents the mortar mixed with a lower amount of steel fibers.

It can be observed in **Fig. 19** that, after 120 seconds of induction heating, for the case of the asphalt mortar with 100 S/m of electrical conductivity, the surface temperature is higher than with 1 S/m (lower amount of steel fibers). This finding supports the observations made by previous researches (*15*), where the induction heating efficiency appears to be proportional to the volume of the inductive particles added in the asphalt mixes.

The amount of steel fibers can also influence the thermal gradient inside the asphalt mortar, **Fig. 19**. For example, for the case of asphalt mortar with 100 S/m of electrical conductivity, the temperature decreases faster inside the mortar, than the case 1 S/m. This thermal gradient difference is caused by the skin effect. When a inductive asphalt mortar has a high electrical conductivity, the alternating magnetic field induces electric currents which are concentrated on the surface of the inductive asphalt mortar. The high concentration of the electric currents leads to a higher heat generation at the surface of the inductive asphalt mortar. Therefore the asphalt mortar with higher electrical conductivity (e.g., 100 S/m) has a higher temperature at the surface but a lower temperature inside the material.

In **Fig. 20**, the effect of thermal conductivity and heat capacity of inductive asphalt mortars is also presented. The parametric analyses are done for inductive asphalt mortar with two different heat capacities (e.g., 875 and 925 J/(kg·K)), four different thermal conductivities (e.g., 0.5, 0.7, 0.9, 1.1 W/(m·K)), while the electrical conductivity of the compared mortars is constant (100 S/m). By comparing to **Fig. 19**, it can be concluded that the impact of the thermal properties of the asphalt mortar on the temperature distribution is not of the same importance with the effect of electrical conductivity.

Effect of Operational Parameters

The numerical results in **Fig. 21** show that the distance between the induction coil and the inductive mortar can influence significantly the heat generation in the inductive asphalt mortar. By increasing the coil distance from 50 mm to 100 mm to the mortar surface, it leads to 50% reduction of the temperature at the surface of the asphalt mortar. This means that for surface induction heating coil closer to the surface is more efficient one at larger distance from the surface of the asphalt mortar. Moreover, the tendency is similar for the materials with different electrical conductivity values.

The power and the frequency of the alternating magnetic field of the induction machine are two important operational parameters that can influence significantly the induction heating efficiency of the inductive asphalt mortar. **Fig. 21** shows the comparison of the effect of the power and the frequency of the induction coil on the

temperature distribution inside the inductive asphalt mortar. It can be observed that, at the same frequency (e.g., 30 kHz), higher machine power results in higher temperatures generated in the material over the whole height.

On the other hand, the frequency of the magnetic field is another important operation parameter. It can be seen that, at constant voltage (e.g., 550 V), the lower frequency of 30 kHz leads to higher maximum surface temperature than the higher frequency of 64 kHz. The distribution of the temperature within the cross-section of the inductive asphalt mortar shows the same tendency for the both cases.

5. Conclusions

The findings of this research were within the efforts to enhance the induction heating of asphalt mixes preparing simultaneously materials with improved mechanical performance during their service. Also, the valuable findings of this research show that it is possible to optimize the necessary tools and equipment needed for the implementation of the induction technology for heating and subsequently healing asphalt pavements. Based on the results presented in this paper, the following conclusions can be made:

- The increase of inductive particles contributes to the enhancement of the electrical and thermal conductivity of asphalt mastic and mortar as well. The utilization of steel fibers has significant improvement on the electrical conductivity of asphalt mortar than the one with iron powder. Moreover, combining steel fibers and iron powder within the mortars, the thermal conductivity is slightly higher than using only steel fibers as inductive particles.
- When steel fibers are added in the asphalt mortar, the tensile strength is improved and the fatigue life is extended. Similar mechanical response is obvious also by combining iron powder and steel fibers.
- The induction heating efficiency is increased when iron powder and steel fibers are added independently to a certain limit, where the temperature does not increase anymore. Apart from the highest induction heating efficiency, asphalt mortars have similar induction healing capacity with mortars with steel fibers when iron powder is mixed.
- Finally, the application of numerical simulations to evaluate the effective properties of inductive asphalt mixes and the different operational conditions of induction heating is proved to be a very effective tool, capable to perform analysis without conducting time consuming and costly experiments. The 3D induction heating numerical model enables to calibrate the model parameters to perform more realistic heating simulations for asphalt concrete mixes.

Acknowledgements

The authors would like to thank Heijmans-Breijn for its financial support on this project. Gratitude is also expressed to K. Kwakernaak and N. Zhong at Delft University of Technology for the SEM and C-Therm TCi thermal testing.

References

1. P. Bazin, J. Saunier, Deformation, fatigue and healing properties of asphalt mixes, *Proc., 2nd International Conference on the Structural Design of Asphalt Pavements*, Ann. Arbor, Mich., (1967) 553-569.
2. D.N. Little, A. Bhasin, Exploring mechanisms of healing in asphalt mixes and quantifying its impact. In *Self-Healing Materials: An Alternative Approach to 20 Centuries of Materials Science* (S. van de Zwaag, ed.), Springer Series in Materials Science, Vol. 100, Springer, Dordrecht, Netherlands, 2007, pp. 205-218.
3. B. Kim, R. Roque, Evaluation of healing property of asphalt mixes, In *Transportation Research Record: Journal of the Transportation Research Board, No. 1970* (2006) 84-91.
4. A. García, Self-healing of open cracks in asphalt mastic, *Fuel*, Vol. 93 (2012) 264-272.
5. E. Schlangen, Other materials, applications and future developments in self-healing phenomena in cement-based materials, M. E. Rooij, et al., Editors, RILEM Series: State-of-the-Art Reports, 2013, pp. 241-256.
6. eurobitume.eu/bitumen/facts-and-stats (accessed 6.7.16)

7. S.B. Chan, B. Lane, T. Kazmierowski, W. Lee, Pavement preservation: a solution for sustainability, *Transportation Research Record, No. 2235* (2011) 36-42.
8. D.S. Decker, *Best practices for crack treatment for asphalt pavement*, NCHRP Report 784 Transportation Research Board of the National Academies, Washington, D.C., 2014.
9. A. García, E. Schlangen, M. van de Ven, Q. Liu, A simple model to define induction heating in asphalt mastic, *Construction and Building Materials*, Vol. 31 (2012) 38-46.
10. A. Garcia, E. Schlangen, M. van de Ven, Two ways of closing cracks on asphalt concrete pavement: microcapsules and induction heating, *Key Engineering Materials*, Vol. 417-418 (2010) 573-576.
11. A. Garcia, E. Schlangen, M. van de Ven, Q. Liu, Electrical conductivity of asphalt mastic containing conductive fibers and fillers, *Construction and Building Materials*, Vol. 23 (2009) 3175-3181.
12. Q. Liu, A. Garcia, E. Schlangen, M. van de Ven, Induction healing of asphalt mastic and porous asphalt concrete, *Construction and Building Materials*, Vol. 25 (2011) 3746-3752.
13. Q. Liu, E. Schlangen, M. van de Ven, Induction healing of porous asphalt concrete, *In Transportation Research Record, No 2305* (2012) 95-101.
14. www.selfhealingasphalt.blogspot.com (accessed 6.7.16)
15. A. Garcia, J. Norambuena-Contreras, M.N. Partl, Experimental evaluation of dense asphalt concrete properties for induction heating purposes, *Construction and Building Materials*, 46 (2013) 48-54.
16. A. Garcia, J. Norambuena-Contreras, M.N. Partl, P. Schuetz, Uniformity and mechanical properties of dense asphalt concrete with steel wool fibers, *Construction and Building Materials*, Vol. 43 (2013) 107-117.
17. A. Menozzi, A. Garcia, M.N. Partl, G. Tebaldi, P, Schuetz. Induction healing of fatigue damage in asphalt test samples, *Construction and Building Materials*, Vol. 74 (2015) 162-168.
18. H. Huang, T.D. White, Dynamic properties of fiber-modified overlay mixture, *Transportation Research Record, No. 1545* (1996) 98-104.
19. K.E. Kaloush, K.P. Biligiri, W.A. Zeiada, M.C. Rodezno, J.X. Reed, Evaluation of fiber-reinforced asphalt mixes using advanced material characterization tests, *Journal of Testing and Evaluation*, Vol. 38, No. 4 (2010) 1-12.
20. Y.X. Zhong, X.L. Wang, M.L. Liao, Experiment research on performance of low-temperature crack resistance of reinforced asphalt mixes, *Advanced Materials Research*, Vol. 163-167 (2010) 1128-1133.
21. H. Kim, K. Sokolov, L.D. Poulikakos, M.N. Partl, Fatigue evaluation of porous asphalt composites with carbon fiber reinforcement polymer grids, *Trasportation Research Record*, *No. 2116* (2009) 108-117.
22. R.C. Mesquita, J.P.A. Bastos, 3D finite element solution of induction heating problems with efficient time-stepping, *IEEE Transactions of Magnetics*, Vol. 27, No. 5 (1991) 4065-4068.
23. A. Boadi, Y. Tsuchida, T. Todaka, M. Enokizono, Designing of suitable construction of high-frequency induction heating coil by using finite-element method, *IEEE Transactions on Magnetics*. Vol. 41, No. 10 (2005) 4048-4050.
24. Z. Wang, W. Huang, W. Jia, Q. Zhao, Y. Wang, W. Yan, 3D Multifields FEM computation of transverse flux induction heating for moving-strips, *IEEE Transactions on Magnetics*. Vol. 35, No. 3 (1999) 1642-1645.
25. *COMSOL. AC/DC Module* – User's Guide. Version 4.4. 2013.
26. *COMSOL. Heat Transfer Module* – User's Guide. Version 4.4. 2013.
27. *Simpleware*. ScanIP, +ScanFE, 2011.
28. S. Wu, P. Pan, F. Xiao, Conductive asphalt concrete: A review on structure design, performance and practical applications, *Journal of Intelligent Material Systems and Structures.* 2013.
29. T.J. Ahmed, D. Stavrov, H.E.N. Bersee, A. Beukers, Induction welding of thermoplastic composites - an overview, *Composite Part A.: Applied Science and Manufacturing*, Vol. 37 (2006) 1638-1651.
30. E. Rapoport, Y. Pleshivtseva, *Optimal control of induction heating processes*. Taylor and Francis Group, 2007.
31. P. Ahmedzade, B. Sengoz, Evaluation of steel slag coarse aggregate in hot mix asphalt concrete, Journal of Hazardous Materials, 165 (2009) 300-305.
32. B. Huang, J. Cao, Z. Chen, X. Shu, W. He, Laboratory investigation into electrically conductive HMA mixtures, Journal of the Association of Asphalt Paving Technologists, Vol. 75 (2006) 1235-1253.
33. P. Park, Y. Rew, A. Baranikumar, Controlling conductivity of asphalt concrete with graphite, Texas A&M Transportation Institute College Station, Report No SWUTC/14/600451-00025-1, 2014.
34. S. Wu, L. Mo, Z. Shui, Z. Chen, Investigation of the conductivity of asphalt concrete containing conductive fillers, Carbon, 43(7) (2005) 1358-1363.
35. X.M. Liu, S.P. Wu, Research on the conductive asphalt concrete's piezoresistivity effect and its mechanism, *Construction and Building Materials*, 23(8) (2009) 2752-2756.
36. X. Liu, S. Wu, Study on the graphite and carbon fiber modified asphalt concrete, *Construction and Building Materials*, 25 (2011) 1807-1811.
37. H. Zhang, X.H. Wu, X.L. Wang, Conductivity mechanism of asphalt concrete with the PANI/PP compound conductive fiber, *Materials Science Forum*, 689 (2011) 69-73.

38. R.N. Traxler, The evaluation of mineral powders as fillers for asphalt, Proc. Assoc. Asphalt Paving Technologists, 8 (1937) 60-67.
39. D.A. Anderson, W.H. Goetz, Mechanical behaviour and reinforcement of mineral filler-asphalt mixtures, Proc. Assoc. Asphalt Paving Technologists, 42 (1973) 37-66.
40. W.G. Buttlar, D. Bozkurt, G.G. Al-Khateeb, A.S. Waldhoff, Understanding asphalt mastic behaviour through micromechanics, *Transportation Research Record, No. 1681* (1999) 157-169.

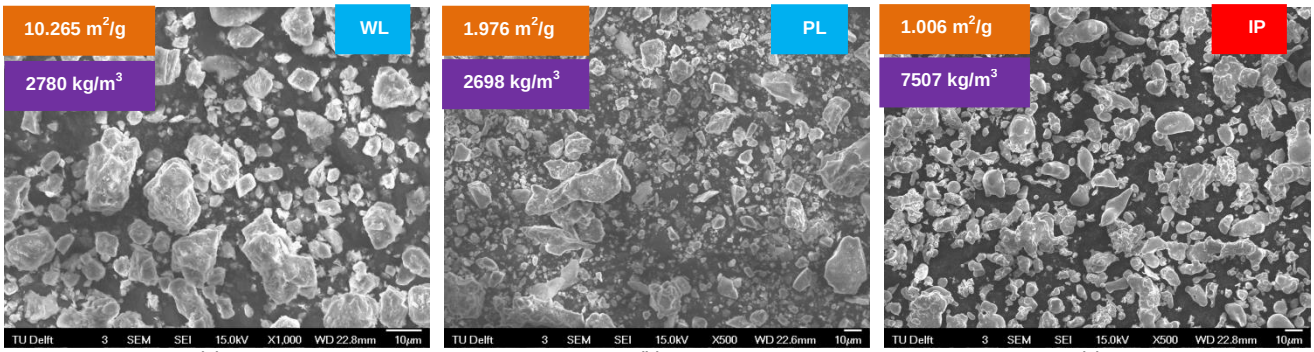

(a) (b) (c)

FIGURE 1 High magnification SEM SEI images of filler-sized particles with their physical properties; (a) WL, (b) PL and (c) IP

TABLE 1 Composition of inductive asphalt mastics

Type of mastic	Density of mastic (gr/m^3)	Mineral filler WL (gr)	Mineral filler PL (gr)	Iron powder IP (gr)
F100.P0	1.594	50.40	7.10	0.00
F95.P5	1.646	47.88	6.75	7.79
F90.P10	1.683	45.36	6.39	15.58
F85.P15	1.730	42.84	6.04	23.37
F80.P10	1.844	40.32	5.68	31.16
F75.P25	1.957	37.80	5.33	38.95
F50.P50	2.243	25.20	3.55	77.90
F25.P75	2.455	12.60	1.78	116.85
F0.P100	2.796	0.00	0.00	155.80
F100.P25	2.361	50.40	7.10	38.95

MA: asphalt mastic, F: mineral filler, P: iron powder, bitumen (gr): 42.5

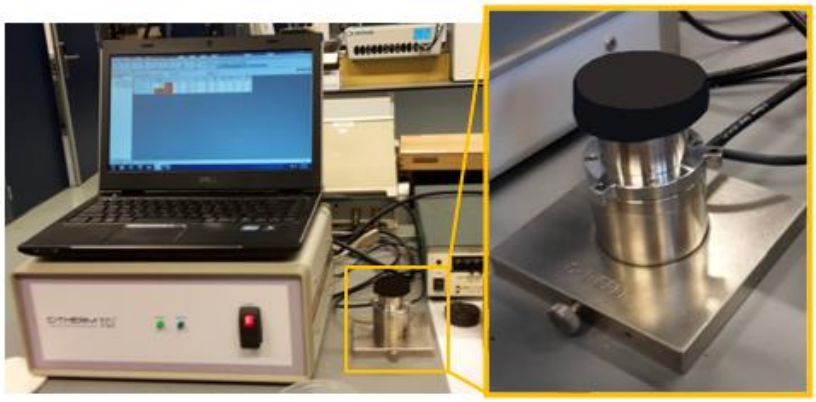

FIGURE 2 TCi analyzer and specimen during thermal measurement

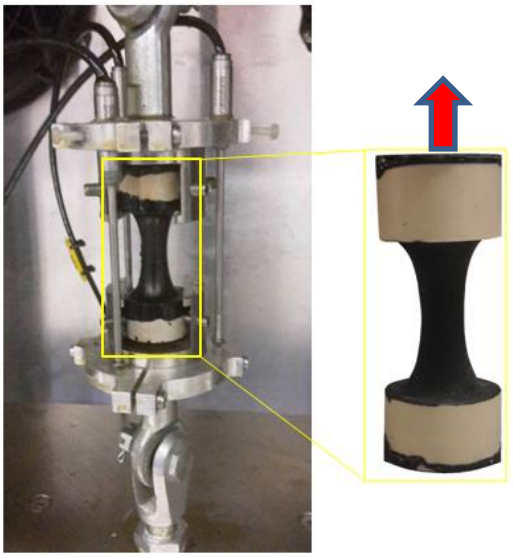

FIGURE 3 The frame and asphalt mortar specimen

FIGURE 4 Induction heating machine used at laboratory

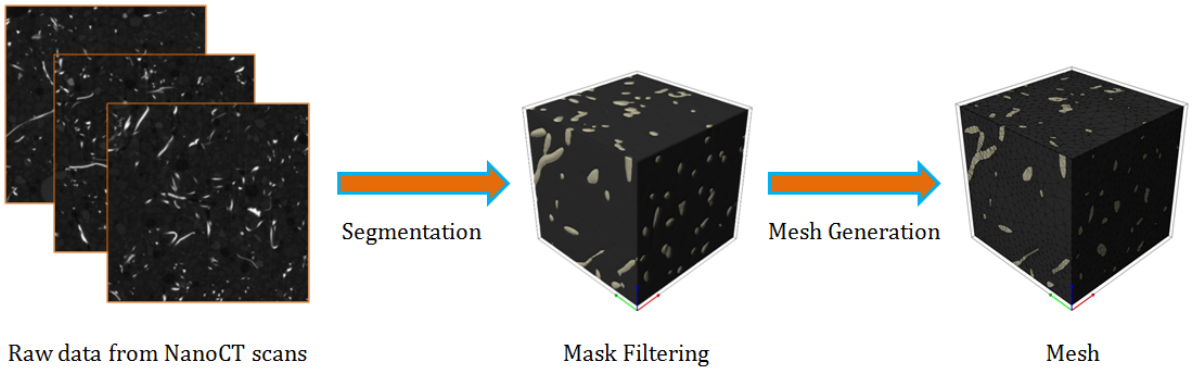

FIGURE 5 Overview of 3D image data post processing

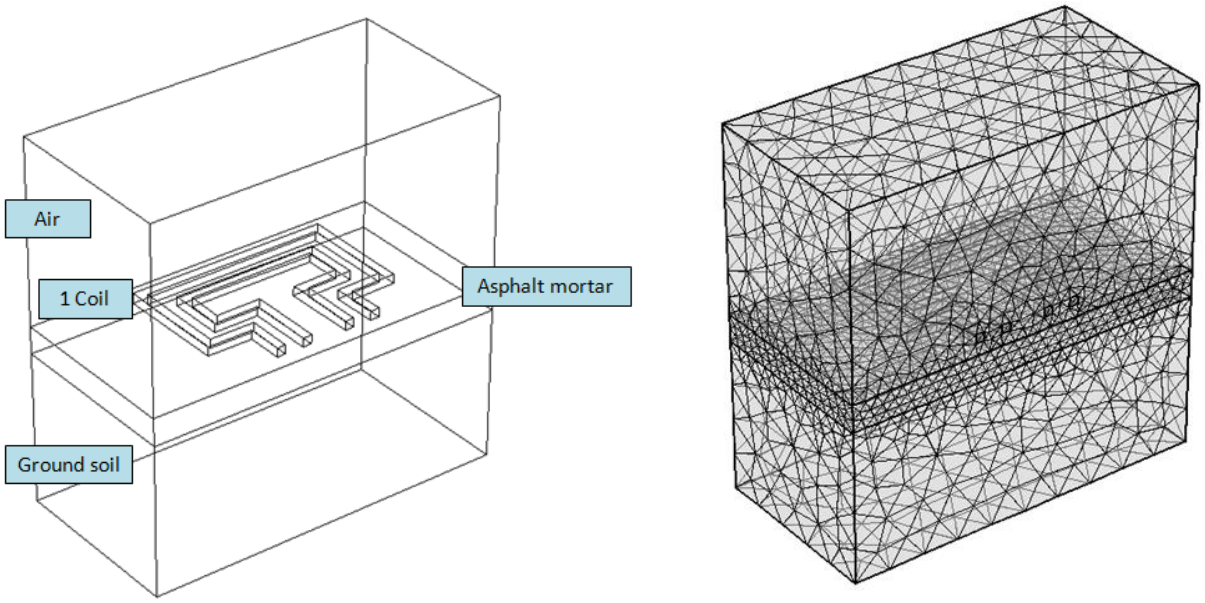

(a) (b)

FIGURE 6 Schematic of (a) one coil and (b)the relative mesh refinements

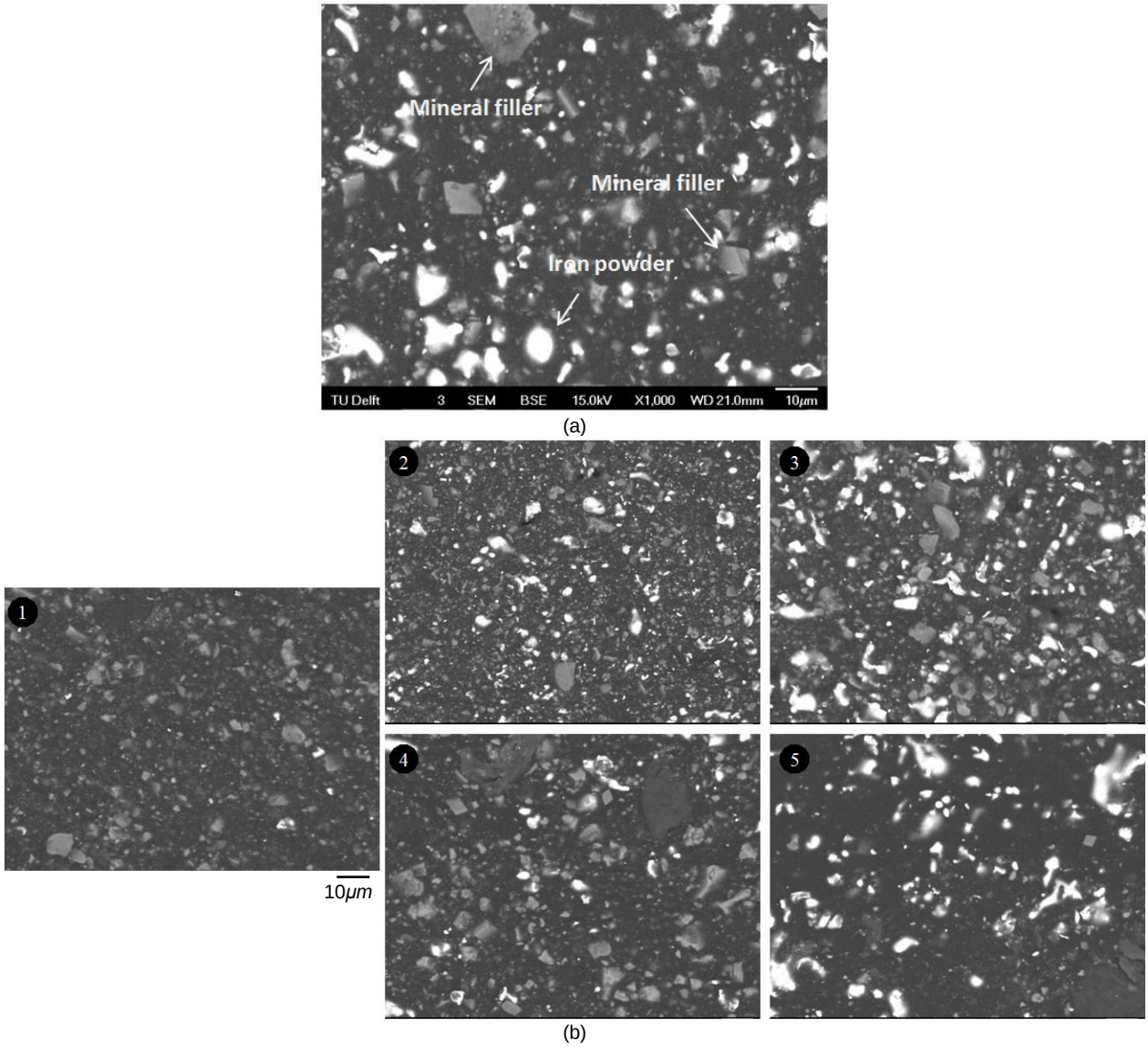

FIGURE 7 SEM BSE (a) image of a inductive asphalt mastics with iron powder and (b) images of inductive asphalt mastics demonstrating the influence of replacing mineral filler with iron powder on the micro-morphology: (1) F100.P0, (2) F100.P25, (3) F100.P50, (4) F75.P25 and (5) F50.P50

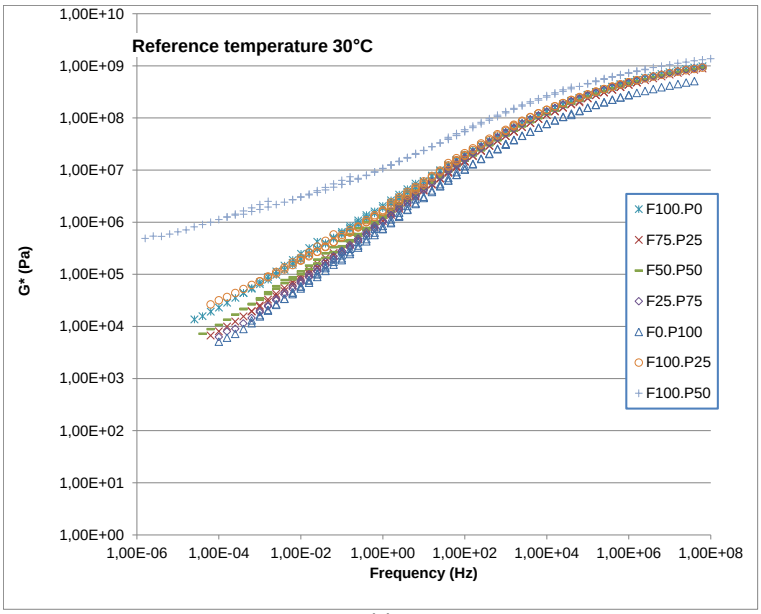

(a)

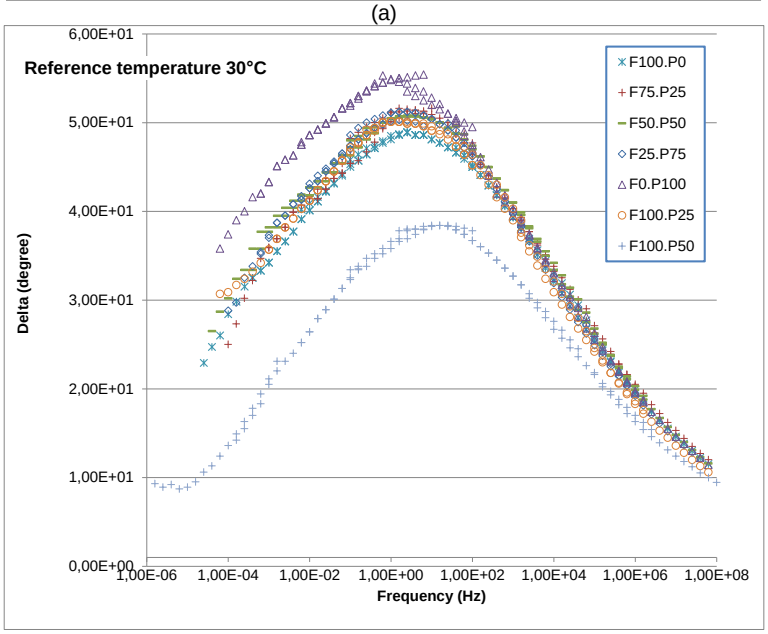

(b)

FIGURE 8 (a) Complex modulus and (b) phase angle master-curves for asphalt mastics produced with and without replacing part of mineral filler with iron powder

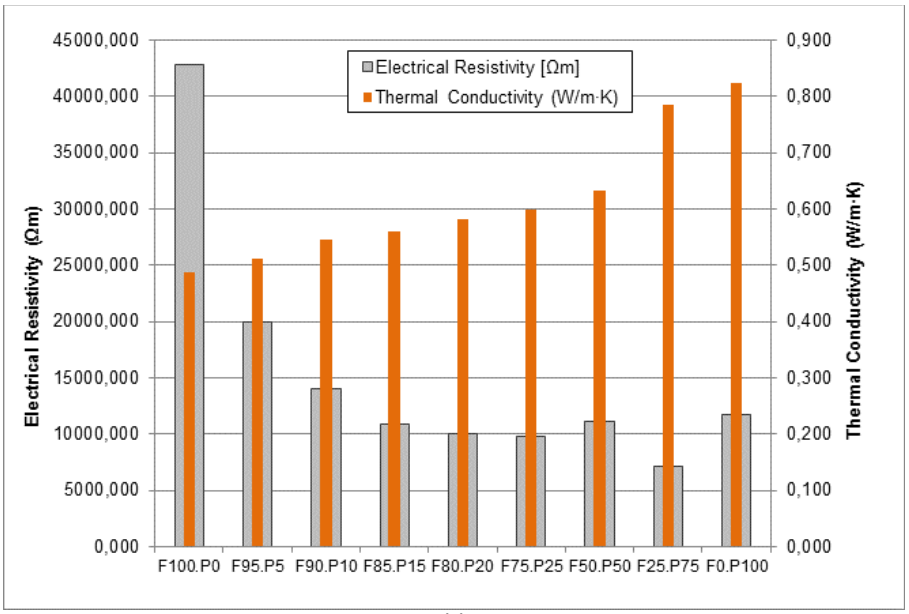

(a)

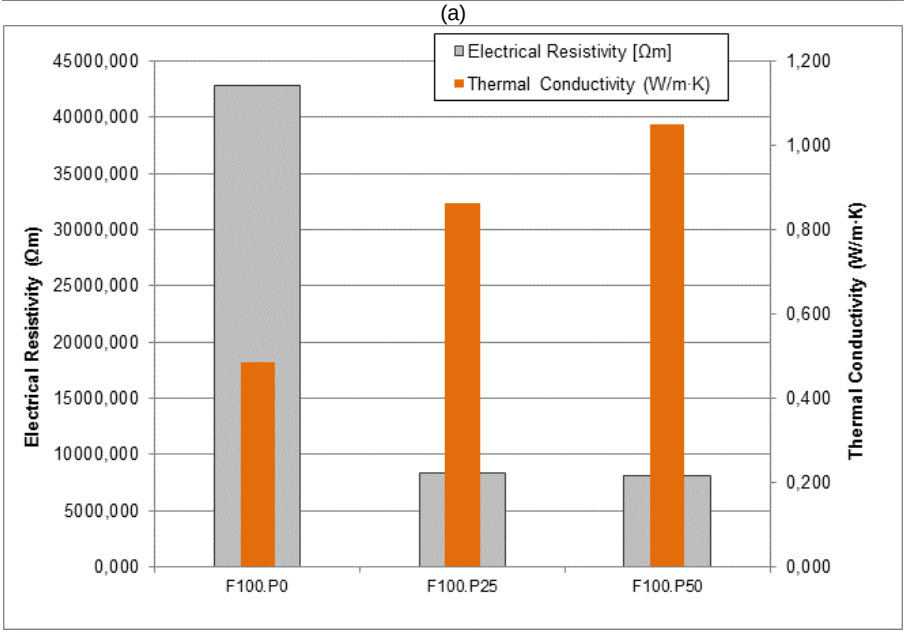

(b)

FIGURE 9 Effect of the volume content of iron powder on the electrical resistivity and thermal conductivity of asphalt mastics (a) after replacing mineral filler with iron powder and (b) without replacing mineral filler with iron powder at 20 ^{o}C

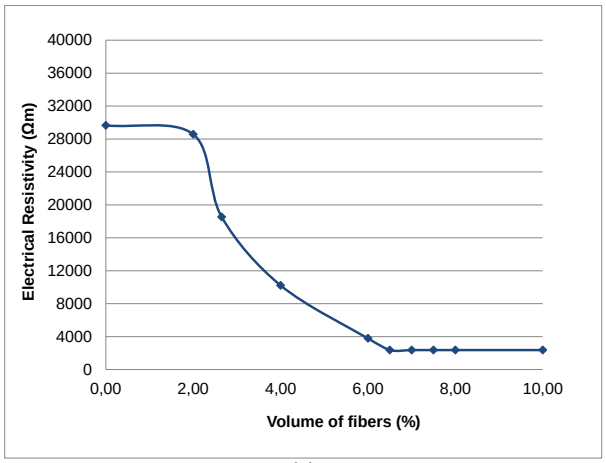

(a)

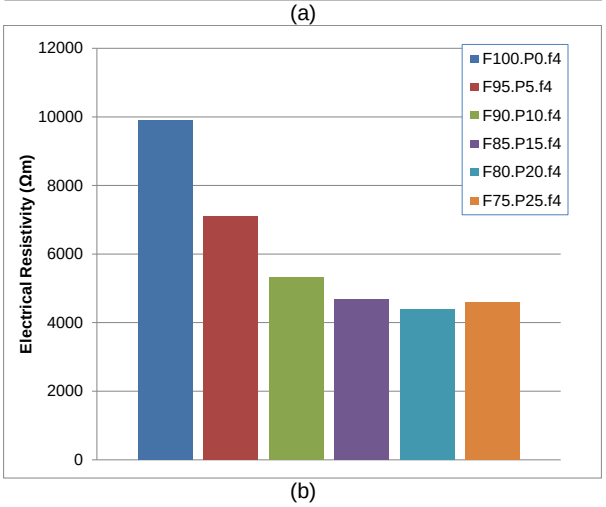

(b)

FIGURE 10 Effect of (a) the volume content of steel fibers and of (b) iron powder after substituting mineral filler with iron on the electrical resistivity of asphalt mortars at 20 ^{o}C

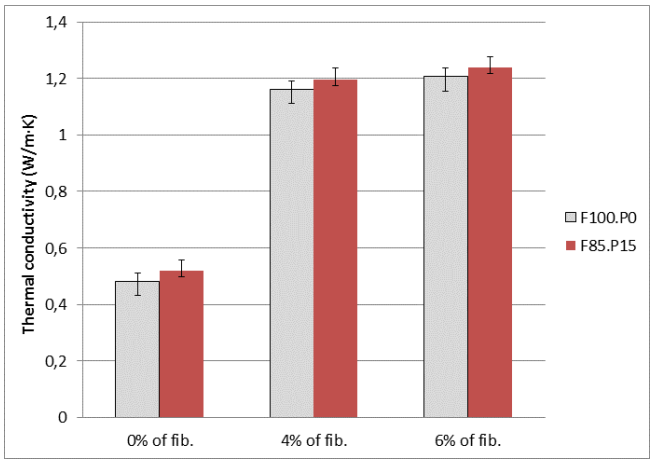

FIGURE 11 Effect of the volume content of steel fibers on the thermal properties of asphalt mortar with and without substituting mineral filler with iron powder at 20 ^{o}C

745

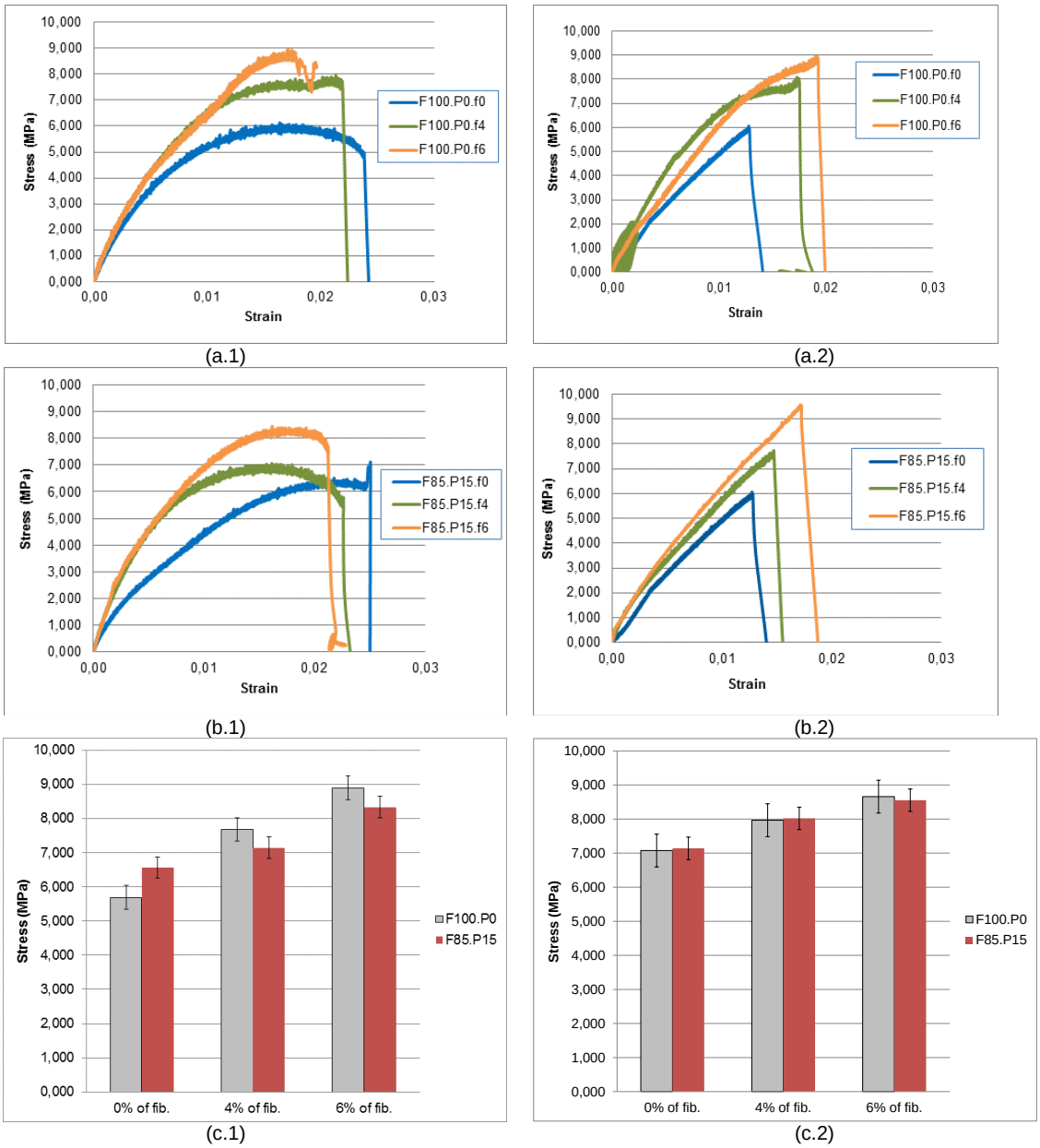

746 **FIGURE 12** The total graphs with the tensile strength of asphalt mortars: displacement rate (c.1) 0.0275
747 mm/s and (c.2) 0.05 mm/s at -10 ^{o}C
748

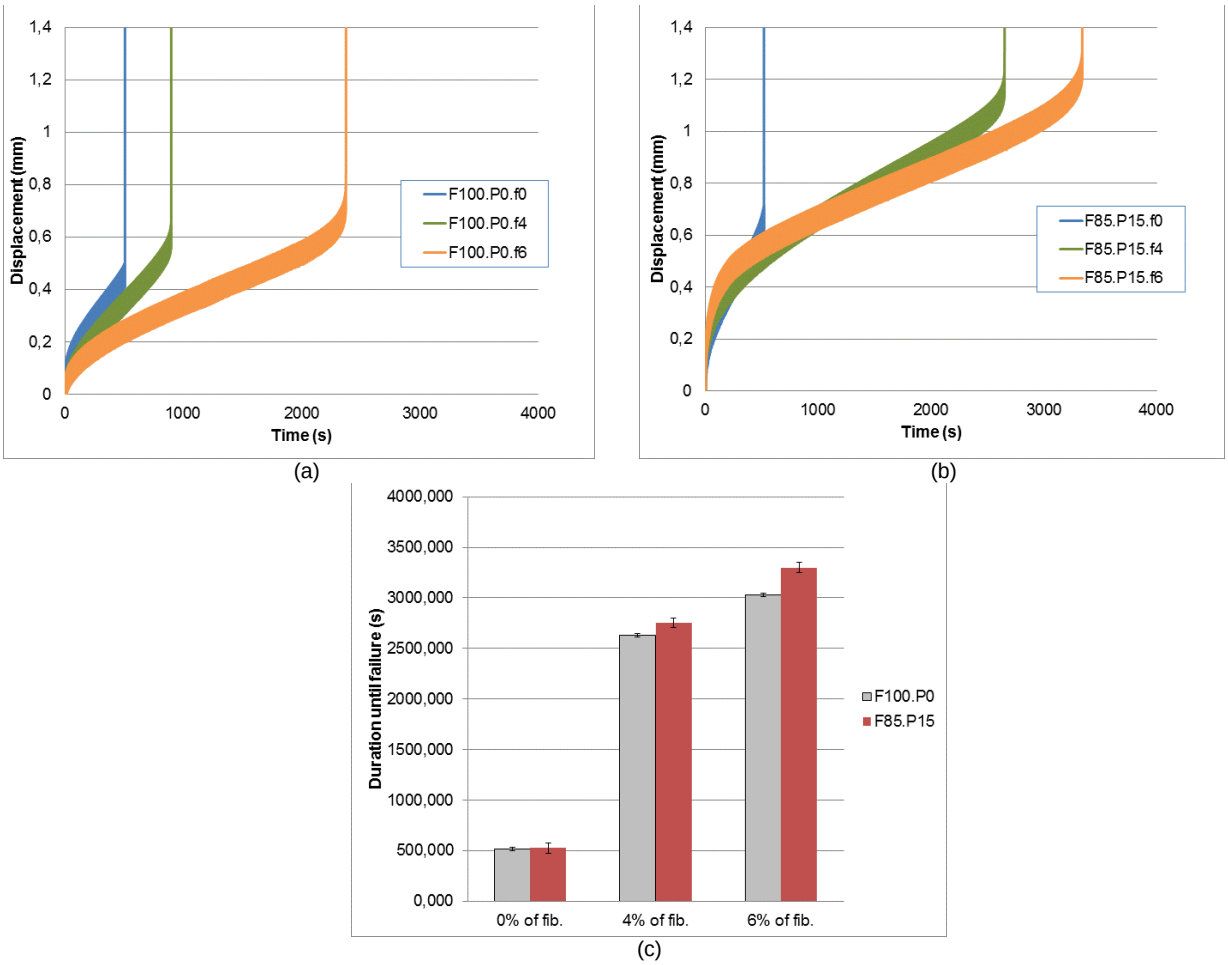

749 **FIGURE 13** Influence of steel fibres on fatigue performance of asphalt mortars (a) without and (b) with iron
750 powder, and (c) the total graph with the fatigue life of different mortars at -10 ^{o}C
751

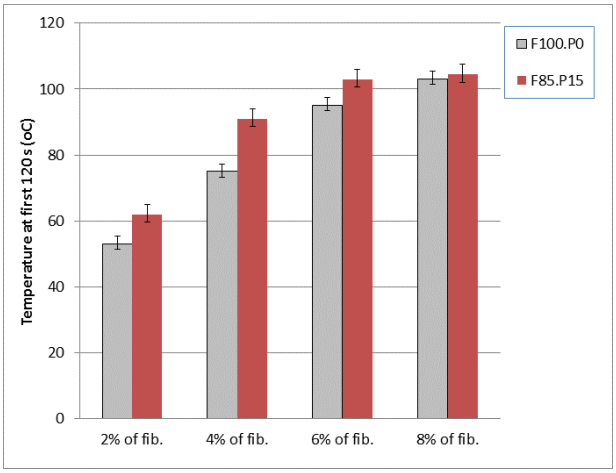

752
753 **FIGURE 14** Temperature reached after 120 seconds induction heating for asphalt mortar with constant
754 volume of steel fibers and different volumes of iron powder

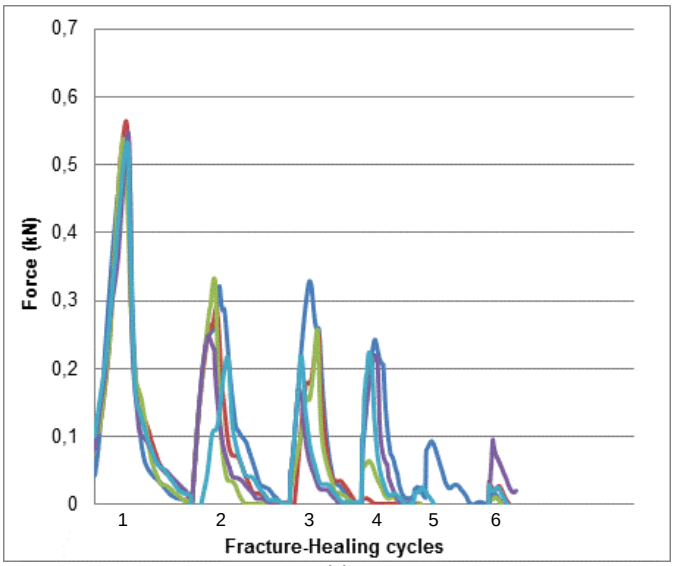

(a)

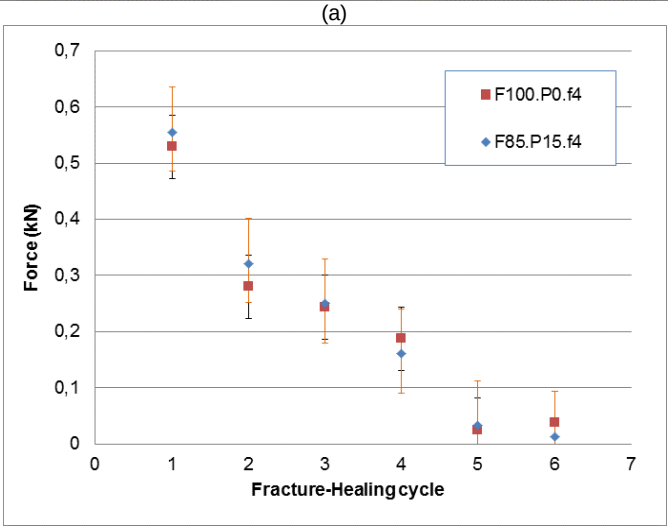

(b)

FIGURE 15 (a) Stress-strain curves for asphalt mortar containing 4% of steel fibers and (b) strength comparison for two types of asphalt mortars at -10 ^{o}C

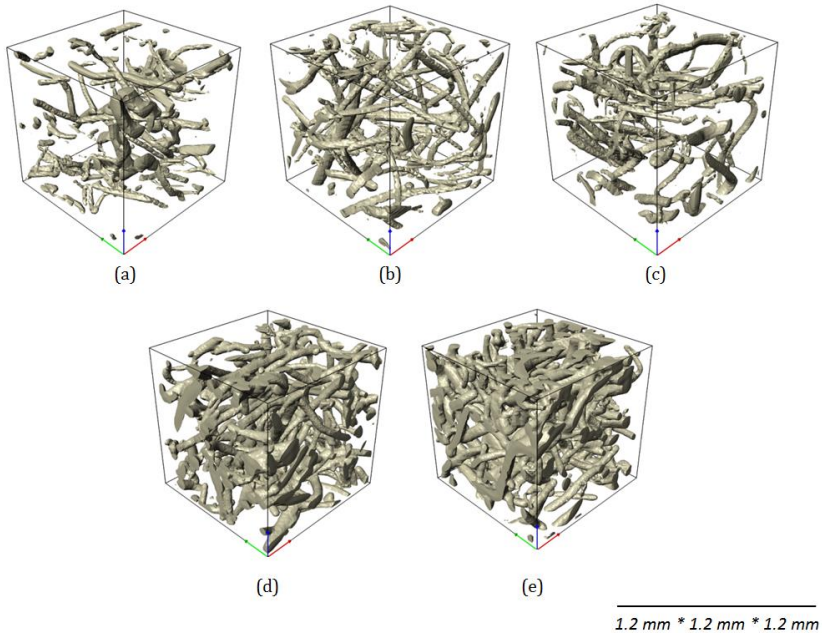

FIGURE 16 Reconstructed images after segmenting the NanoCT-scans for the inductive asphalt mortars with different steel fibers content; (a) 3.4 %, (b) 4.7 %, (c) 5.2 %, (d) 6.8 % and (e) 13.3 % of steel fibers

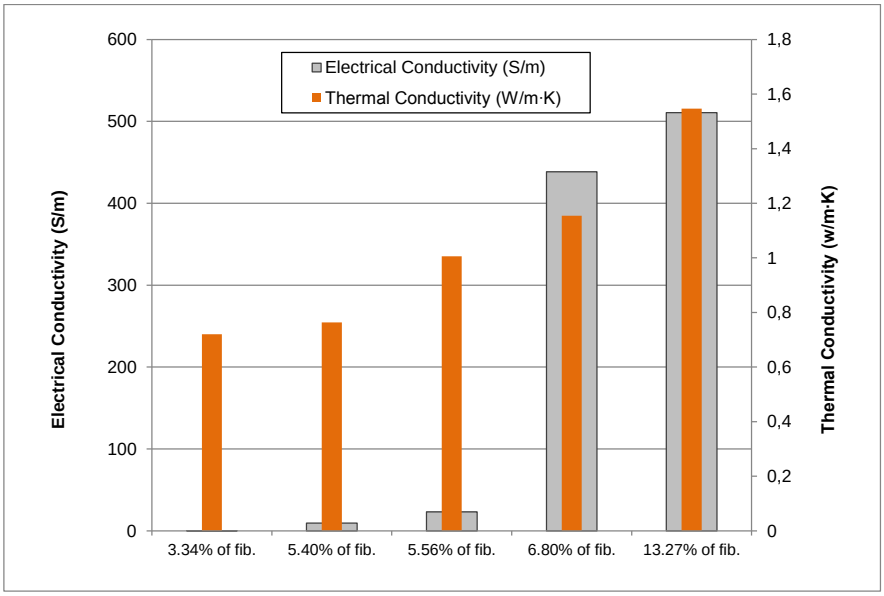

FIGURE 17 Numerically determined effective (a) electrical and (b) thermal conductivity of different asphalt mortars

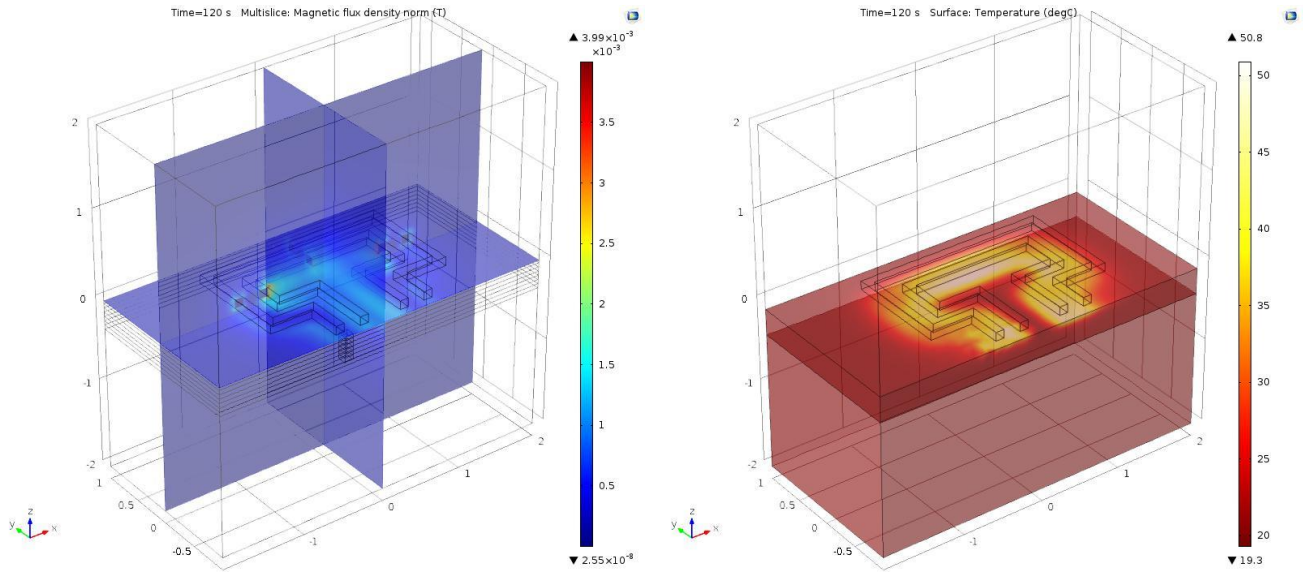

(a) (b)

FIGURE 18 (a) Magnetic flux density and (b) temperature distribution at the end of induction heating

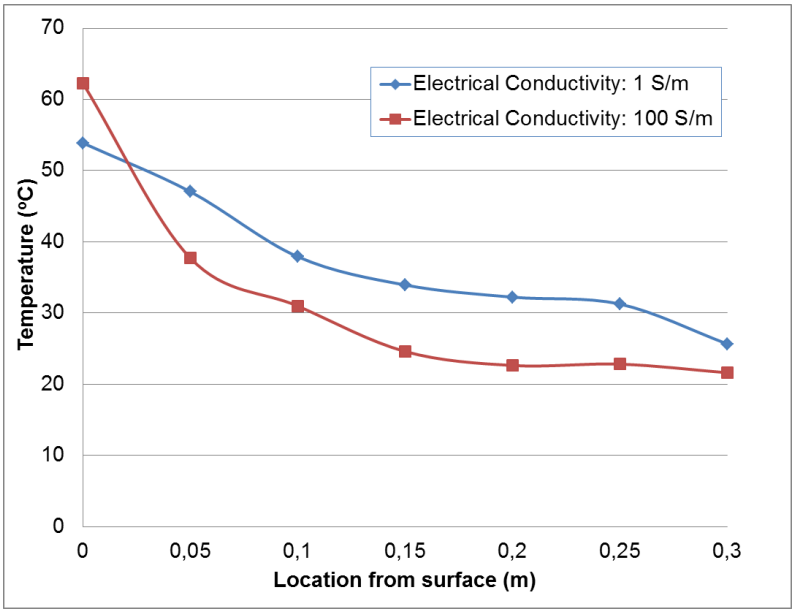

FIGURE 19 Influence of the electrical conductivity of the inductive asphalt mortars on temperature distribution (induction time 120s)

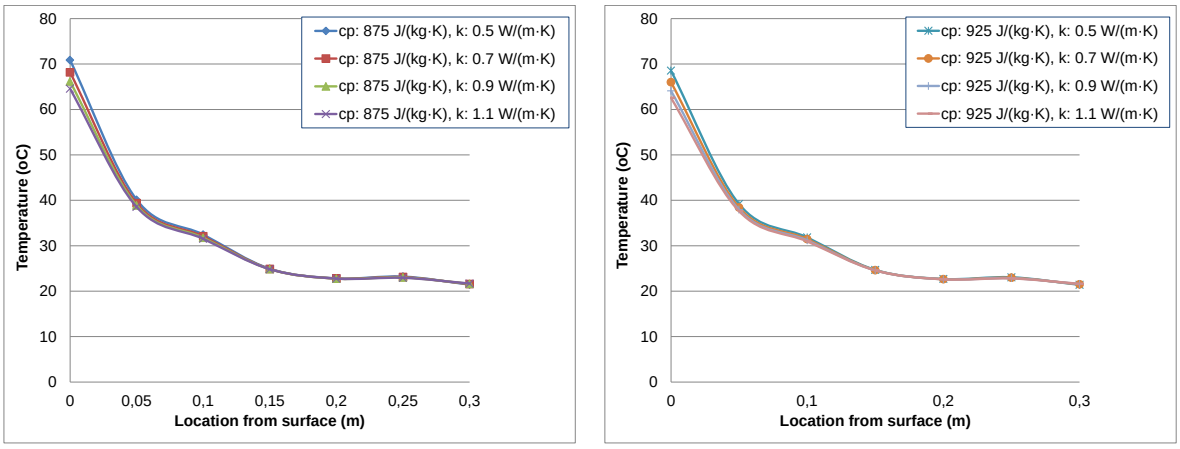

(a) (b)

774 **FIGURE 20** Influence of the thermal conductivity and heat capacity of the inductive asphalt mortars on
775 temperature distribution (electrical conductivity 100 S/m, induction time 120s)
776

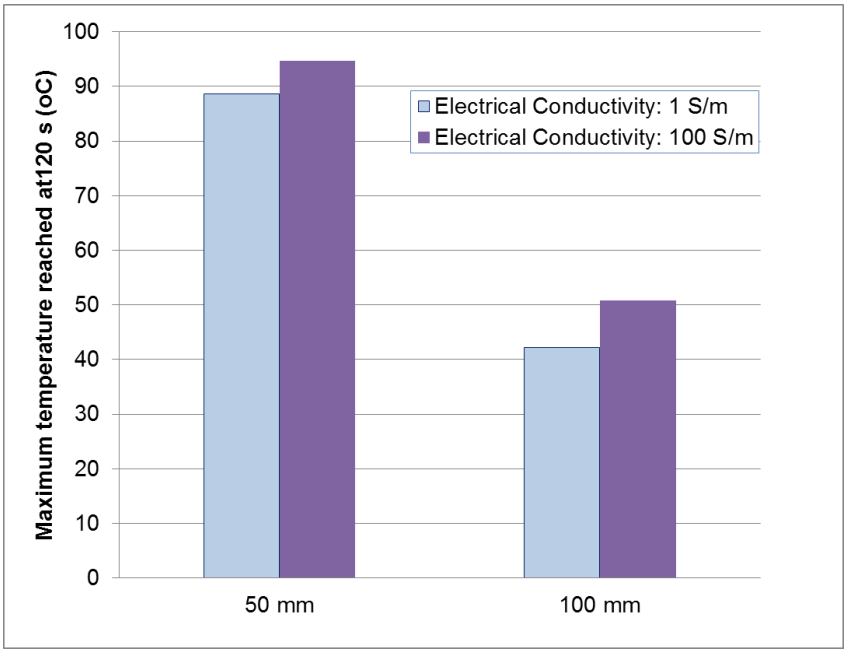

777
778 **FIGURE 21** Maximum temperature generated by the single coil system at the different electrical
779 conductivities at the different coil distances to the inductive asphalt mortar
780

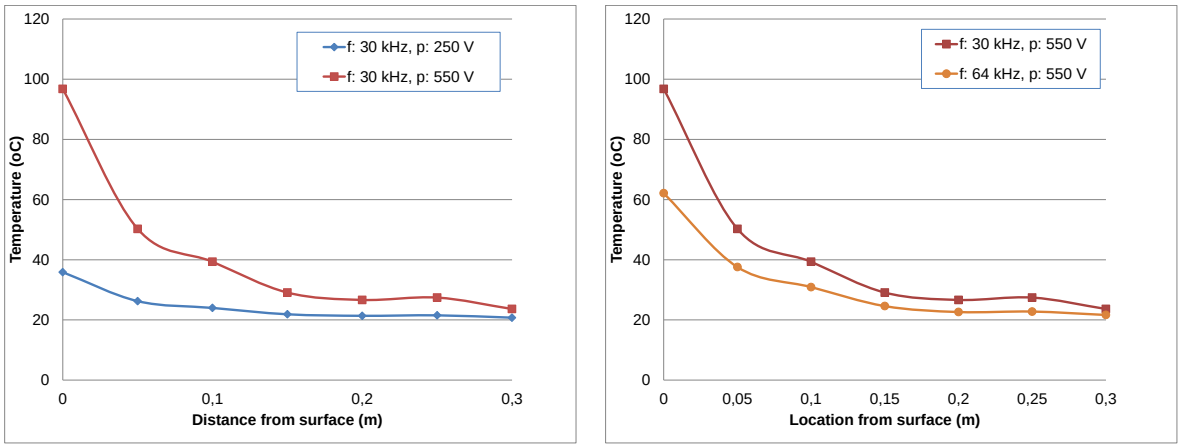

781 **FIGURE 22** Influence of (a) the supplied power and (b) the frequency of induction coil (electrical conductivity
782 100 S/m, induction time 120s)